J|A|C|S ARTICLES

Published on Web 12/15/2009

Alternative Selective Oxidation Pathways for Aldehyde Oxidation and Alkene Epoxidation on a SiO_2-Supported Ru−Monomer Complex Catalyst

Mizuki Tada,*,† Satoshi Muratsugu,† Mutsuo Kinoshita,† Takehiko Sasaki,‡ and Yasuhiro Iwasawa§

Institute for Molecular Science, 38 Nishigo-Naka, Myodaiji, Okazaki, Aichi 444-8585, Japan, Department of Complexity Science and Engineering, Graduate School of Frontier Sciences, The University of Tokyo, Kashiwanoha, Kashiwa, Chiba 277-8561, Japan, and Department of Applied Physics and Chemistry, The University of Electro-Communications, Chofu, Tokyo 182-8585, Japan

Received September 23, 2009; E-mail: mtada@ims.ac.jp

Abstract: We have prepared a novel Ru-mononer complex supported on a SiO_2 surface by using a Ru-monomer complex precursor with a *p*-cymene ligand, which was found to be highly active for the selective oxidation of aldehydes and the epoxidation of alkenes using O_2. The structure of the supported Ru catalyst was characterized by means of FT-IR, solid-state NMR, diffuse-reflectance UV/vis, XPS, Ru K-edge EXAFS, and DFT calculations, which demonstrated the formation of isolatedly located, unsaturated Ru centers behind a *p*-cymene ligand of the Ru-complex precursor. The site-isolated Ru-monomer complex on SiO_2 achieved tremendous TONs (turnover numbers) for the selective oxidation of aldehydes and alkenes; e.g. TONs of 38,800,000 for selective isobutyraldehyde (IBA) oxidation and 2,100,000 for *trans*-stilbene epoxidation at ambient temperature, which are among the highest TONs in metal-complex catalyzes to our knowledge. We also found that the IBA sole oxidation with an activation energy of 48 kJ mol^{-1} much more facile than the *trans*-stilbene epoxidation with an activation energy of 99 kJ mol^{-1} was completely suppressed by the coexistence of *trans*-stilbene. The switchover of the selective oxidation pathways from the IBA oxidation to the *trans*-stilbene epoxidation was explained in terms of energy profiles for the alternative selective oxidation pathways, resulting in the preferential coordination of *trans*-stilbene to the Ru-complex at the surface. This aspect gives an insight into the origin of the efficient catalysis for selective epoxidation of alkenes with IBA/O_2.

1. Introduction

Many useful chemicals are produced by heterogeneous solid catalysts in industrial processes, and the merits of heterogeneous catalysts are not only the separation of catalysts and products from reaction media but also their high durability and unique activities derived from the site-isolation and structure of catalytically active sites at solid surfaces. Relationship among the structure, organized environment, and catalytic property of surface species tells us how to establish a new strategy for rational design of heterogeneous catalysts.

Supporting organic and inorganic metal complexes on surfaces is a promising way to produce molecularly regulated structures of active metal sites at surfaces, and various surface metal structures can be arranged by stepwise structural transformations in a controllable manner.[1−3] Metal complex attachment and subsequent thermal and chemical treatments often produce novel unsaturated active metal centers, which are unique and highly active for catalytic reactions.[4−14] Chemical bonding between metal complexes and a support surface prevents gathering the unsaturated active metal species, and hence the resultant site isolation provides a stabilization effect on such labile structures. The coordinatively unsaturated metal center may provide an efficient reaction pathway in the coordination sphere via adsorption of multiple reactants on the metal center.

Recently, we have succeeded in preparing novel unsaturated Ru-diamine monomer complexes on a SiO_2 surface, which are active for selective oxidation reactions of alkenes and cycloal-

† Institute for Molecular Science.
‡ The University of Tokyo.
§ The University of Electro-Communications.

(1) Iwasawa, Y. *Adv. Catal.* **1987**, *35*, 187.
(2) Hartley, F. R. *Supported Metal Complexes*; Reidel: Dordrecht, 1985.
(3) Iwasawa, Y. *Tailored Metal Catalysts*; Reidel: Dordrecht, 1986.
(4) Iwasawa, Y. *Acc. Chem. Res.* **1997**, *30*, 103.
(5) Thomas, J. M.; Raja, R.; Lewis, D. W. *Angew. Chem., Int. Ed.* **2005**, *44*, 6456.
(6) Tada, M.; Iwasawa, Y. *Chem. Commun.* **2006**, 2833.
(7) Notestein, J.; Katz, A. *Chem.—Eur. J.* **2006**, *12*, 3954.
(8) McMorn, P.; Hutchings, G. *J. Chem. Soc. Rev.* **2004**, *33*, 108.
(9) Sheldon, R. A.; Wallau, M.; Arends, I. W. C.; Schuchardt, U. *Acc. Chem. Res.* **1998**, *31*, 485.
(10) Corma, A.; Garcia, H. *Adv. Synth. Catal.* **2006**, *348*, 1391.
(11) Coperet, C.; Basset, J. M. *Adv. Synth. Catal.* **2007**, *349*, 78.
(12) Fierro-Gonzalez, J. C.; Kuba, S.; Hao, Y. L.; Gates, B. C. *J. Phys. Chem. B* **2006**, *110*, 13326.
(13) Yamaguchi, K.; Yoshida, C.; Uchida, S.; Mizuno, N. *J. Am. Chem. Soc.* **2005**, *127*, 530.
(14) Bianchini, C.; Dal Santo, V.; Meli, A.; Moneti, S.; Moreno, M.; Oberhauser, W.; Psaro, R.; Sordelli, L.; Vizza, F. *J. Catal.* **2003**, *213*, 47.

 © 2010 American Chemical Society

kanes using O_2.[15,16] A *p*-cymene ligand of the supported Ru-diamine complex can be extracted to create the coordinatively unsaturated active Ru center at the surface by two novel methods that we have developed: (1) the reaction-induced selective elimination of the *p*-cymene ligand[15] and (2) the photoinduced selective elimination of the *p*-cymene ligand.[16] Although the formation of unsaturated metal species is generally endothermic and necessitated by compulsory evacuation at high tempreture,[17−21] we succeeded in producing the unsaturated active Ru center in conjunction with the exothermic reaction of reactant conversion and subsequent ligand exchange on a supported Ru complex.[15] The exothermic reaction of isobutyraldehyde (IBA) to isobutyric acid promoted the endothermic elimination of a *p*-cymene ligand from the supported Ru complex. The unsaturated Ru complex thus formed on the surface exhibited high activity and selectivity for epoxidation of alkenes. On the other hand, the irradiation of the SiO_2-supported Ru complex with UV light brought about the selective elimination of a *p*-cymene ligand and the immobilization of the Ru complex at double sites on the SiO_2 surface. The doubly immobilized Ru complex was active for the photooxidation of cycloalkanes using O_2 as an oxidant.[16]

In this contribution, we report the characterization and alternative selective oxidation catalysis (aldehyde oxidation and alkene epoxidation) of the SiO_2-supported unsaturated Ru-monomer complex produced by the reactant-induced catalyst activation. The selective alkene epoxidation using IBA and O_2 on the Ru-monomer complex proceeded with a tremendous TON (turnover number) (e.g., 2.1×10^6 for *trans*-stilbene epoxidation) without catalytic IBA oxidation, which may be of interest, because the catalytic oxidation of IBA itself with O_2 in the absence of *trans*-stilbene proceeded more rapidly with the larger TON of 3.9×10^7 and TOF (turnover frequency) of 1.6×10^3 s^{-1} at ambient temperature, which are both among the highest values in metal complex catalysis, to our knowledge. The switchover of the reaction pathways from the aldehyde oxidation to the alkene epoxidation is also discussed in terms of energy profiles for the alternative selective oxidation pathways at the surface to promote the selective epoxidation of alkenes.

2. Experimental Section

Catalyst Preparation. Preparation of a Diamine Ligand $H_2NCH_2CH_2NHSO_2C_8H_7$. A CH_2Cl_2 solution (15 mL) of 4-vinylbenzensulfonyl chloride (5 mL) was dropped into 5 mL of ethylene diamine dissolved in 10 mL of CH_2Cl_2, and the mixture was stirred for 3 h. CH_2Cl_2 (200 mL), H_2O (100 mL), and HCl/H_2O (2 M, 200 mL) were added to the solution, and the water layer was washed with CH_2Cl_2 twice. After filtration, the water layer was neutralized by KOH solution (2 M, pH 9−10) and extracted with 150 mL of CH_2Cl_2 three times. The organic layers were dried with Na_2SO_4, and filtrated, and the solvents were evaporated. Elemental analysis (calculated % for $C_{10}H_{14}N_2O_2S$ (observed %)): C 53.08 (52.88), H 6.24 (6.22), N 12.38 (12.25). ^{1}H NHR ($CDCl_3$): 2.17 (brm, 2H; NH_2), 2.81 (m, 2H; CH_2), 2.98 (m, 2H; CH_2), 5.43 (d, 1H; CH=CH_2), 5.87 (d, 1H; CH=CH_2), 6.74 (dd, 2H; CH = CH_2), 7.52 (d, 2H; C_6H_4), 7.82 (d, 2H; C_6H_4).

Synthesis of Ru Precursor [(*p*-Cymene)Ru{$H_2NCH_2CH_2NHSO_2C_8H_7$}Cl] (A). The diamine ligand $H_2NCH_2CH_2NHSO_2C_8H_7$ (226 mg, 1 mmol) dissolved in CH_2Cl_2/CH_3OH (1/1 15 mL) and $NaOCH_3$ (1 mmol) in CH_3OH (0.5 mL) were slowly added to a CH_2Cl_2 solution (20 mL) of Ru_2(*p*-cymene)$_2Cl_4$ (306 mg, 0.5 mmol). The mixture was stirred for 3 h under N_2 atmosphere, and then the solvent was evaporated. The residue was dissolved in CH_2Cl_2/diethylether (2/1, 30 mL), and after filtration the solution was reduced to 2 mL under vacuum. *n*-Hexane (15 mL) was added, and the precipitate was dried under vacuum. Elemental analysis (calculated % for $C_{20}H_{27}ClN_2O_2RuS$ H_2O (observed %)): C 46.73 (46.59), H 5.69 (5.65), N 5.45 (5.39). ^{1}H NHR ($CDCl_3$, 298 K): 1.11 (d, 6H; CH(CH_3)$_2$), 2.01 (s, 3H; CH_3 (*p*-cymene)), 2.12 (brm, 4H; NCH_2), 2.64 (sept, 1H; CH(CH_3)$_2$), 5.08 (d, 1H; CH=CH_2) 5.13 (brd, 2H; CH (*p*-cymene)), 5.40 (d, 2H; CH (*p*-cymene)), 5.64 (d, 1H; CH=CH_2), 6.50 (dd, 1H; CH = CH_2), 7.23 (d, 2H; C_6H_4), 7.67 (d, 2H; C_6H_4). ^{13}C NMR ($CDCl_3$): 18.56, 22.53 (CH_3, *p*-cymene), 30.39 (CH, *p*-cymene), 47.27, 48.51 (NCH_2), 81.30 (CH, *p*-cymene), 96.12 (C, *p*-cymene), 102.21, 115.40, 125.81, 127.47, 135.92, 139.36, 142.80 (C_6H_4−CH=CH_2).

Preparation of a Supported Ru Complex (C). SiO_2 (1.5 g, Aerosil 200; Degussa) was calcined at 673 K for 2 h and refluxed in a solution of *p*-styryltrimethoxysilane (0.11 mmol) in anhydrous toluene at 383 K for 18 h under N_2. The modified SiO_2 was filtrated and then dried under vacuum. The amount of grafted *p*-styryl moiety was 0.23 nm^{-2}. The prepared Ru precursor (**A**) (38 mg, 0.074 mmol) was reacted with SiO_2 functionalized with *p*-styryltrimethoxysilane in anhydrous $CHCl_3$ (20 mL) in the presence of AIBN, then refluxed at 333 K for 24 h under N_2. The obtained SiO_2-supported catalyst was filtrated, washed with $CHCl_3$, and dried under vacuum. Loading of Ru complex was 0.4 wt % by XRF. A supported Ru complex with 2.7 wt % of Ru loading was prepared with the similar procedure.

Preparation of an Unsaturated Ru Complex on SiO_2 (D). The supported Ru complex (**C**) (1.5 g, Ru 0.4 wt %) was suspended in anhydrous CH_2Cl_2 (20 mL). Neat isobutyraldehyde (0.2 mL) was added to the suspension, and the mixture was stirred for 3 h under O_2 atmosphere, accompanied with change of the color from orange to pale black. Then the obtained catalyst was filtrated, washed with CH_2Cl_2, and dried under vacuum.

Catalyst Characterization. XPS. XPS spectra were recorded on a Rigaku XPS-7000 apparatus at a base pressure of 6×10^{-6} Pa. The X-ray source, voltage, and current were Mg Ka, 10 kV, and 30 mA, respectively. Binding energies were referred to C 1s of 284.8 eV.

^{1}H and ^{13}C NMR. ^{1}H and ^{13}C NMR spectra in a liquid phase were obtained on JNM-AL400 spectrometers at 400 MHz in $CDCl_3$ with TMS of an internal standard. Solid state ^{13}C MAS NMR spectra (MAS rate = 6 kHz) were recorded with a Chemagnetics CMX-300 spectrometer operating at 75.5 MHz. ^{13}C MAS NMR spectra with cross-polarization (CP) were acquired with contact time 5.0 ms. The rotor spin rate was 6 kHz, with delay time of 2 s. Hexamethylbenzene (17.17 and 176.46 ppm) was used as an external standard for the calibration of chemical shifts.

Ru K-edge EXAFS. EXAFS spectra at Ru K-edge were measured in a transmission mode at 15 K at the NW10A station of the PF-AR ring at High Energy Accelerator Research Organization (KEK). The energy and current of electrons in the storage ring were 6.5 GeV and 50−60 mA, respectively. X-rays from the storage ring were monochromatized by Si(311) channel cut crystals. Ionization chambers filled with pure Ar and Kr gases were used to monitor the incident and transmitted X-rays, respectively. EXAFS

(15) Tada, M.; Coquet, R.; Yoshida, M.; Kinoshita, M.; Iwasawa, Y. *Angew. Chem., Int. Ed.* **2007**, *46*, 7220.
(16) Tada, M.; Akatsuka, Y.; Yang, Y.; Sasaki, T.; Kinoshita, M.; Motokura, K.; Iwasawa, Y. *Angew. Chem., Int. Ed.* **2008**, *47*, 9252.
(17) Asakura, K.; Bando, K. K.; Iwasawa, Y.; Arakawa, H.; Isobe, K. *J. Am. Chem. Soc.* **1990**, *112*, 9096.
(18) Izumi, Y.; Chihara, H.; Yamazaki, H.; Iwasawa, Y. *J. Phys. Chem.* **1994**, *98*, 594.
(19) Asakura, K.; Noguchi, Y.; Iwasawa, Y. *J. Phys. Chem. B* **1999**, *103*, 1051.
(20) Taoufik, M.; Santini, C. C.; Candy, J.-P.; de Mallmann, A.; Basset, J. M. *J. Am. Chem. Soc.* **1996**, *118*, 4167.
(21) Humblot, F.; Didillon, D.; Lepeltier, F.; Candy, J. P.; Corker, J.; Clause, O.; Bayard, F.; Basset, J. M. *J. Am. Chem. Soc.* **1998**, *120*, 137.

spectra were analyzed with the UWXAFS package.[22] Threshold energy E_0 was tentatively set at the inflection point of the absorption edge, and background was subtracted by the AUTOBK program. k^3-Weighted EXAFS oscillations were Fourier transformed into R-space. Curve-fitting analysis was carried out using the FEFFIT program in the R-space. k-Range for the Fourier transformation was 30−140 nm^{-1}. Fitting parameters were coordination numbers (CN), interatomic distances (R), Debye−Waller factors (σ), and a correction-of-edge energy (ΔE_0). The same ΔE_0 was used for all the shells in a sample. Phase shifts and backscattering amplitudes for Ru−C, Ru−N, and Ru−Cl bonds were calculated by the FEFF8 code.[23] The coefficient of multiphoton effect (S_0^2) was fixed as 1.0 for the fitting.

DFT Calculations. Structural optimizations based on DFT were performed using the Gaussian03 package.[24] The PBE0 hybrid functional[25] was employed with the DGDZVP basis set.[26] The DGDZVP basis set is equivalent to Pople's Hartree−Fock optimized 6-31G* basis set.[27] Unlike the popular B3LYP,[28] PBE0 is a nonempirical hybrid GGA functional and provides remarkable results for a number of physicochemical observables without any adjustable parameters.[29,30] Relative energies of singlet and triplet spin states were assessed to obtain the lowest energy structures. It was found that the system with the Ru complex interacting with O_2, IBA, and *trans*-stilbene favors the triplet state throughout the reaction paths. Transition states were optimized by the synchronous transit-guided quasi-Newton (STQN) method, and they were confirmed by the existence of a single negative frequency.

Catalytic Oxidation Reactions. Selective Catalytic Oxidation of Aldehydes. Each catalyst was suspended in a CH_2Cl_2 solution under 101.3 kPa of oxygen in a closed glass reactor equipped with a mechanical stirrer. Aldehyde oxidation reactions were carried out at 288 K by the addition of neat aldehyde to the suspension (Ru/aldehyde = 1/200 in a molar ratio). Reactants and products were analyzed by GC (Shimadzu GC-17A) and GC-MS (Shimadzu GC-2010) at an appropriate interval. Activation energies (E_a) were calculated using reaction rates in the temperature range of 281−313 K, and reaction orders were examined in the aldehyde concentration range of 0.025−0.4 M.

Catalytic Epoxidation of Alkenes. Each catalyst was suspended in a CH_2Cl_2 solution under 101.3 kPa of oxygen in a closed glass reactor equipped with a mechanical stirrer. Alkene epoxidation reactions were conducted at 298 K by the addition of an alkene reactant and IBA to the suspension (Ru/IBA/alkene = 1/200/200 in a molar ratio). Reactants and products were analyzed by GC (Shimadzu GC-17A) and GC-MS (Shimadzu GC-2010) at an appropriate interval. Activation energies (E_a) were estimated in the temperature range of 283−314 K, and the reaction orders to aldehyde and alkene were also determined.

Stereoselective Epoxidation of Cholesterol Benzoate. The epoxidation of 5,6-double bond in cholesteryl benzoate (0.5 mmol) was carried out using *m*-CPBA (0.5 mmol) in CH_2Cl_2 5 mL under N_2 atmosphere at 288 K. The same epoxidation was performed on the supported Ru catalyst (**D**) (Ru 0.4 wt %, 60 mg) with cholesteryl benzoate (0.5 mmol) in CH_2Cl_2 5 mL (Ru/cholesteryl benzoate/IBA = 1/200/200) under the atmospheric pressure of O_2 at 288 K. After 3 and 24 h, the products of α-epoxide and β-epoxide were analyzed by ^{1}H NMR (H_6 of α-epoxide: 2.9 ppm and that of β-epoxide: 3.1 ppm).[31]

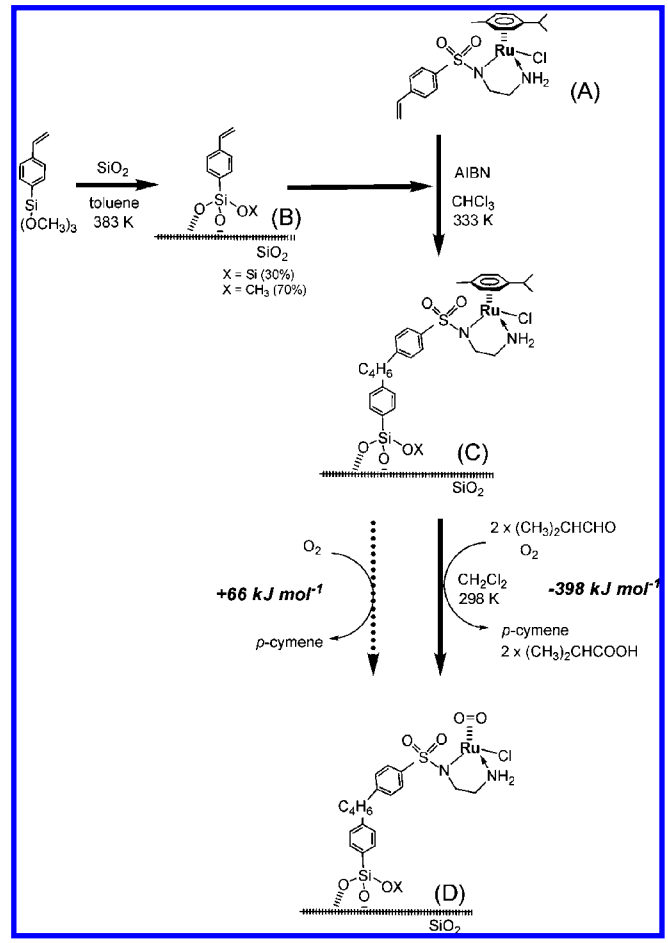

Figure 1. Structures of a SiO_2-supported Ru catalyst for selective oxidation.

Iodometry Analysis. NaI was dissolved in 2-propanol and 10% acetic acid was added to the solution. The supported Ru catalyst (**D**) was immediately added to the mixture after its catalytic reaction and subsequent filtration, and refluxed at 333 K for 0.5 h. The mixture was titrated using a 0.1 N sodium thiosulfate solution.

3. Results and Discussion

3.1. Catalytically Active Structure of the Supported Ru-Monomer Complex on a SiO_2 Surface. The SiO_2-supported unsaturated Ru-monomer complex was prepared via step-by-step reactions in three steps as illustrated in Figure 1. The Ru complexes synthesized/transformed on the surface have been characterized by ^{13}C and ^{29}Si solid-state NMR, FT-IR, diffuse-reflectance UV/vis, Ru $3d_{5/2}$ XPS, Ru K-edge EXAFS, and hybrid DFT calculations. Here, the structure of the active Ru complex supported on SiO_2 is discussed, summarizing our previous results and presenting new data.[15] *p*-Styryltrimethoxysilane was tethered on the surface of SiO_2, whose density at the surface was controlled to be a given density in the range of 0.1 − 0.8 nm^2. ^{13}C and ^{29}Si solid-state NMR revealed that the *p*-styryl moiety was tethered on the SiO_2 surface (species **B** in Figure 1; and in a and d of Figure 2). The appearance of new

(22) Stern, E. A.; Newville, M.; Ravel, B.; Yacoby, Y.; Haskel, D. *Physica B* **1995**, *208&209*, 117.
(23) Ankudinov, A. L.; Ravel, B.; Rehr, J.; Conradson, S. D. *Phys. Rev. B* **1998**, *58*, 7565.
(24) Frisch, M. J., et al., *GAUSSIAN 03*, Rev. C. 02; Gaussian Inc.: Wallingford, CT, 2004. Complete ref available in the Supporting Information.
(25) Perdew, J. P.; Burke, K.; Ernzerhof, M. *Phys. Rev. Lett.* **1996**, *77*, 3865.
(26) Sosa, C.; Andzelm, J.; Elkin, B. C.; Wimmer, E.; Dobbs, K. D.; Dixon, D. A. *J. Phys. Chem.* **1992**, *96*, 6630.
(27) Hariharan, P. C.; Pople, J. A. *Chem. Phys. Lett.* **1972**, *66*, 217.
(28) Becke, A. D. *J. Chem. Phys.* **1993**, *98*, 5648.
(29) Adamo, C.; Scuseria, G. E.; Barone, V. *J. Chem. Phys.* **1999**, *111*, 2889.
(30) Scalmani, G.; Bredas, J. L.; Barone, V. *J. Chem. Phys.* **2000**, *112*, 1178.
(31) Yamada, T.; Imagawa, K.; Mukaiyama, T. *Chem. Lett.* **1992**, 2109.

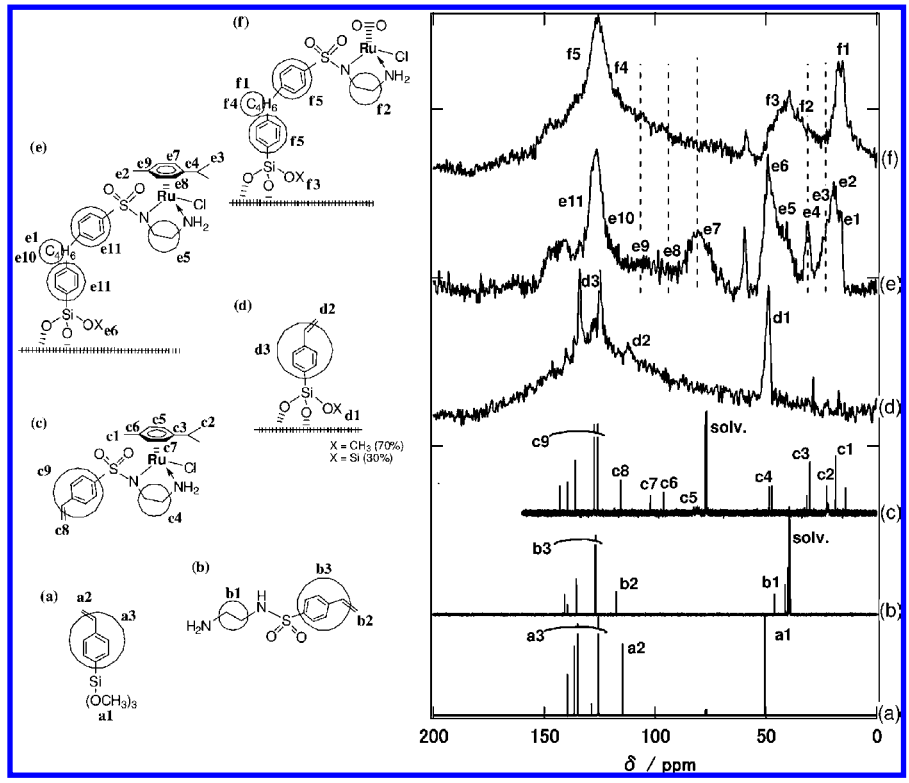

Figure 2. ^{13}C liquid and solid-state NMR spectra of (a) *p*-styryltrimethoxysilane, (b) *N*-sulfonyl-1,2-ethylenediamine, (c) the Ru precursor complex (**A**), (d) the immobilized *p*-styryltrimethoxysilane on SiO_2 (**B**), (e) the supported Ru complex (**C**), and (f) the supported Ru catalyst after the removal of *p*-cymene (**D**). Dotted lines represent peaks attributed to *p*-cymene.

Table 1. Ru Loadings, Released *p*-Cymene Amounts, and XPS Binding Energies of the Homogeneous Ru Precursor Complex (**A**), the Supported Ru Catalysts (**C**) and (**D**)

				XPS binding energy		
catalyst	Ru wt %[a]	Ru wt %[a,b]	detected *p*-cymene/Ru[c]	O 1s[d]	Si 2p[d]	Ru $3d_{5/2}$[d]
Ru complex (**A**)	–	–	–	531.7	–	281.6
supported catalyst (**C**)	0.4	–	–	532.9	103.4	281.6
supported catalyst (**D**)	0.4	0.4	0.88	532.9	103.4	281.9
supported catalyst (**C**)	2.7	–	–	533.0	103.4	281.5
supported catalyst (**D**)	2.7	2.7	0.89	533.0	103.4	282.0

[a] Loading of Ru was measured by XRF. [b] Loading of Ru after the catalytic epoxidation. [c] Free *p*-cymene in the solution of IBA detected by GC. [d] Binding energies were referred to C 1s of 284.8 eV.

peaks at −62 and −54 ppm in ^{29}Si solid-state NMR for species (**B**) in Figure 1 indicated that two or three methoxy moieties of *p*-styryltrimethoxysilane made the interfacial bonds as -Si(-OSi)$_3$ (30%) and −Si(−OSi)$_2$(−OCH$_3$) (70%) as illustrated in Figure 1(species **B**).[15]

Then the Ru-precursor complex with a styryl moiety (**A**), synthesized from the reaction of *N*-surfonyl-1,2-ethylenediamine with $Ru_2(p\text{-cymene})_2Cl_4$,[32] was grafted by a reaction with the styryl moiety of the functionalized SiO_2 (**B**). The reduction of a FT-IR peak intensity at $\nu_{C=C}$ at 1625 cm^{-1} and ^{13}C solid-state NMR peaks at 112.8 ppm and 134.6 ppm (Figure 2) for the styryl C=C groups confirm that the Ru-precursor complex (**A**) was immobilized on the surface via the consumption of the styryl moieties of species **B** as shown in Figure 1 (**C**). UV/vis spectra of (**A**) and (**C**) were observed at 326 nm (Ru d → Ph π) and 447 nm (Cl p → Ru d), indicating that the Ru complex (**A**) was immobilized with retention of its original local coordination structure on the Ru^{2+} site as illustrated in Figure 1 (**C**). XPS binding energies of Ru $3d_{5/2}$ for species A (Ru^{2+}) and species (**C**) were 281.6 and 281.5 eV, respectively, which are almost the same (Table 1). ^{13}C solid-state NMR in Figure 2 and Ru K-edge EXAFS (Table 2) also evidence the similarity of the local coordination structures of the supported Ru complex (**C**) and the precursor complex (**A**).

We found that the coordinating *p*-cymene ligand of the supported complex (**C**) selectively released in the presence of isobutyraldehyde (IBA) and O_2.[15] Hybrid DFT calculations revealed that the simple extraction of the *p*-cymene ligand from (**C**) was endothermic (66 kJ mol^{-1}) and we could not spontaneously produce the unsaturated Ru complex by the elimination of the *p*-cymene ligand by heating under vacuum and N_2. However, when IBA and O_2 existed, the exothermic reaction of IBA and O_2 to form isobutyric acid was concertedly devoted to extract the *p*-cymene ligand of (**C**). The concerted reaction of the energy-gaining IBA conversion and the subsequent *p*-cymene ligand elimination produced the unsaturated active Ru complex (**D**) with aid of the exothermic reaction of 398 kJ mol^{-1}.[15] The *p*-cymene ligand stoichiometrically released and

(32) Haak, K. J.; Hashiguchi, S.; Fujii, A.; Ikariya, T.; Noyori, R. *Angew. Chem.* **1997**, *109*, 297.

Table 2. Curve-fitting analysis for the Ru K-edge EXAFS data measured at 15 K

shell	CN	distance/nm	σ^2/nm^2
Ru Precursor (**A**)[a]			
Ru−Cl	1.0 (fixed)	0.236 ± 0.003	$(2 \pm 3) \times 10^{-5}$
Ru−N	2.0 (fixed)	0.213 ± 0.002	$(-1 \pm 2) \times 10^{-5}$
Ru−C	6.0 (fixed)	0.227 ± 0.021	$(2 \pm 24) \times 10^{-5}$
Supported Complex (**C**)[b]	Ru 2.7 wt %		
Ru−Cl	1.0 (fixed)	0.236 ± 0.006	$(3 \pm 6) \times 10^{-5}$
Ru−N	2.0 (fixed)	0.214 ± 0.002	$(0 \pm 2) \times 10^{-5}$
Ru−C	6.0 (fixed)	0.226 ± 0.023	$(13 \pm 23) \times 10^{-5}$
Supported Complex (**D**)[c]	Ru 2.7 wt %		
Ru−Cl	1.3 ± 1.5	0.234 ± 0.004	$(5 \pm 8) \times 10^{-5}$
Ru−N	2.2 ± 1.5	0.207 ± 0.003	$(1 \pm 2) \times 10^{-5}$
(**D**) after *trans*-stilbene epoxidation[d]	Ru 2.7 wt %		
Ru−Cl	1.5 ± 2.3	0.232 ± 0.006	$(4 \pm 12) \times 10^{-5}$
Ru−N	2.2 ± 1.8	0.206 ± 0.003	$(8 \pm 2) \times 10^{-5}$
Supported Complex (**C**)[e]	Ru 0.4 wt %		
Ru−Cl	1.0 (fixed)	0.238 ± 0.002	$(1 \pm 2) \times 10^{-5}$
Ru−N	2.0 (fixed)	0.214 ± 0.002	$(0 \pm 2) \times 10^{-5}$
Ru−C	6.0 (fixed)	0.230 ± 0.037	$(20 \pm 43) \times 10^{-5}$
Supported Complex (**D**)[f]	Ru 0.4 wt %		
Ru−Cl	1.3 ± 1.5	0.236 ± 0.004	$(2 \pm 9) \times 10^{-5}$
Ru−N	2.0 ± 1.7	0.209 ± 0.003	$(0 \pm 3) \times 10^{-5}$

[a] $k = 30-140$ nm^{-1}, $R = 0.10-0.22$ nm, $\Delta E_0 = 10 \pm 8$, $R_f = 1.74\%$. CNs of Ru−Cl, Ru−N, and Ru−C were fixed. [b] $k = 30-140$ nm^{-1}, $R = 0.10-0.22$ nm, $\Delta E_0 = 10 \pm 9$, $R_f = 2.31\%$. CNs of Ru−Cl, Ru−N, and Ru−C were fixed. [c] $k = 30-140$ nm^{-1}, $R = 0.13-0.24$ nm, $\Delta E_0 = 10 \pm 3$, $R_f = 1.29\%$. [d] $k = 30-140$ nm^{-1}, $R = 0.13-0.24$ nm, $\Delta E_0 = 9 \pm 5$, $R_f = 1.01\%$. [e] $k = 30-140$ nm^{-1}, $R = 0.10-0.22$ nm, $\Delta E_0 = 9 \pm 15$, $R_f = 2.42\%$. CNs of Ru−Cl, Ru−N, and Ru−C were fixed. [f] $k = 30-140$ nm^{-1}, $R = 0.13-0.24$ nm, $\Delta E_0 = 11 \pm 1$, $R_f = 1.14\%$.

89% (2.7 Ru wt% catalyst) and 88% (0.4 Ru wt% catalyst) of the released *p*-cymene were detected in the solution (Table 1). No release of *p*-cymene occurred under N_2 atmosphere instead of O_2 atmosphere where the exothermic oxidation of IBA could not proceed.

After the release of the coordinating *p*-cymene ligand, Ru K-edge EXAFS for the supported Ru complex (**D**) showed that there are three chemical bonds (two Ru−N and one Ru−Cl): Ru−N bonds (coordination number (CN) = 2.2 ± 1.5) at 0.207 ± 0.003 nm and Ru−Cl bond (CN = 1.3 ± 1.5) at 0.234 ± 0.004 nm as shown in Table 2. No Ru−Ru bonding was observed in agreement of a Ru-monomer complex structure immobilized at the surface. All peaks of ^{13}C NMR attributed to the *p*-cymene ligand disappeared as shown in Figure 2 (dotted lines) and there were no significant changes in the chemical shifts of the diamine ligand and its branch before and after the selective elimination of *p*-cymene. On the supported catalyst (**D**) after the removal of *p*-cymene, O_2 was suggested to adsorb on the unsaturated Ru site.[15] When the CH_2Cl_2 solution of *trans*-stilbene and IBA was added to (**D**) under N_2 atmosphere, the formation of *trans*-stilbene oxide (70% of the stoichiometric quantity to Ru) in the solution was observed, indicating that O_2 had been coordinated on the unsaturated Ru site. Furthermore, when we exposed (**D**) to other aldehyde molecules in CH_2Cl_2, no isobutyric acid derived from coordinated IBA was detected in the solution. Thus, it is suggested that O_2 alone coordinates to the unsaturated Ru site of (**D**), but there are neither IBA nor its corresponding peracid species remained as ligands on the unsaturated Ru species (**D**). The modeling by DFT calculations suggested that the side-on coordination structure (**D**) illustrated in Figure 1 was more stable than the coordination structure of end-on-type O_2. Ru $3d_{5/2}$ XPS binding energy was observed as 282.0 eV, which is assigned as Ru^{3+} (Table 1), indicating that the coordinating O_2 on Ru is negatively charged on (**D**).

After the catalytic oxidations on the supported Ru catalyst (**D**), the structure of the unsaturated Ru complex (**D**) remained unchanged as shown in Table 2. The two kinds of chemical bonds of Ru−Cl (coordination number (CN) = 1.5 ± 2.3, bond distance (*d*) = 0.232 ± 0.006 nm) and Ru−N (CN = 2.2 ± 1.8, *d* = 0.206 ± 0.003 nm) were observed, and these structural parameters were almost the same as those for the 3-coordinated unsaturated structure of (**D**). Such kind of unsaturated species easily aggregate in solutions and indeed the elimination of *p*-cymene caused aggregation of the formed unsaturated Ru species in the case of homogeneous Ru-precursor complex (**A**). Low stability of unsaturated metal complexes leading to aggregation or decomposition in solutions prevents from exploiting metal-complex catalysis. The metal-complex attachment on solid surfaces for isolation of the unsaturated metal centers is promising as a powerful platform not only for the dramatic improvement of catalytic activity but also for a better understanding of key issues for selective catalysis by the metal-complex structures. The coordinatively unsaturated metal center can provide an efficient reaction pathway in the coordination sphere via multiple adsorption of plural reactant molecules on the metal center.

3.2. Selective Oxidation of Aldehydes to Corresponding Carboxylic Acids. It was found that the supported Ru complex (**D**) showed tremendous activities for selective aldehyde oxidation to corresponding acids. Table 3 shows the catalytic performances of the IBA oxidation with O_2. At 288 K, the IBA oxidation was hard to proceed in the absence of any Ru catalysts and the support SiO_2 gave no positive effect on the oxidation. RuO_2, $RuCl_3$, $Ru_2(p\text{-cymene})_2Cl_4$, and Ru precursor complex (**A**) were inactive or less selective for the IBA oxidation as shown in Table 3. $Ru_2(p\text{-cymene})_2Cl_4$ converted 94% of IBA to isobutyric acid after 24 h with the acid selectivity of 72%, however the reuse of this homogeneous complex did not produce any products at all. On the other hand, the supported Ru catalyst (**D**) after the elimination of *p*-cymene efficiently promoted the IBA oxidation with good conversion (93%) and selectivity (94%) in 4 h.

Interestingly, although the Ru homogeneous complex (**A**) and the supported catalyst (**D**) showed similar color changes under

Table 3. Catalytic Performances of Various Ru Compounds for the IBA Oxidation[a] to Isobutyric Acid in CH_2Cl_2

catalyst	IBA/Ru	time/h	conversion %	selectivity %
SiO_2[b]		2	0	0
		6	0.5	60
$RuCl_3$[c]	50	3	30	58
	50	24	99	61
RuO_2[c]	50	3	18	65
	50	24	93	64
$Ru_2(p\text{-cymene})_2Cl_4$[c]	50	1	33	72
	50	24	94	72
$Ru_2(p\text{-cymene})_2Cl_4$ (reuse)[c]	50	24	0	0
Ru precursor (**A**)[d]	200	24	0	0
supported Ru catalyst (**D**) (Ru 0.4 wt %)[d]	200	4	93	94
supported Ru catalyst (**D**) (Ru 2.7 wt %)[c]	50	2	90	94

[a] Reagents and conditions: 288 K, CH_2Cl_2 3 mL, O_2 101.3 kPa. [b] SiO_2 35 mg. [c] Ru 6.0×10^{-6} mol. [d] Ru 1.5×10^{-6} mol.

Table 4. Catalytic Performances for Aldehyde Oxidation[a] to Corresponding Carboxylic Acids at 288 K on the SiO_2-Supported Ru-Complex Catalysts (Ru 0.4 wt %) after the Removal of *p*-Cymene

reactant	[aldehyde] (mol/L)	time/h	TON	selectivity/%
isobutyraldehyde	0.10	4	186	94
butyraldehyde	0.10	4	192	100
1-heptanal	0.10	24	186	100
1-octanal	0.10	24	182	100
2-ethylhexanal	0.10	4	194	87
1-decanal	0.10	24	184	98
1-dodecanal	0.10	24	184	88
acetaldehyde	0.10	48	22	100
glutaraldehyde[b]	0.10	5	200	41
cyclohexanecarboxaldehyde	0.10	24	190	90
benzaldehyde	0.10	24	122	100
3-phenylpropionaldehyde	0.10	24	166	85
phenylglyoxal	0.10	24	150	100
p-chlorobenzaldehyde	0.10	24	136	100
2,6-dichlorobenzaldehyde	0.10	24	30	68
isobutyraldehyde[c]	neat	12	38,800,000	94
1-heptanal[c]	neat	48	31,500,000	98
3-phenylpropionaldehyde[d]	4.5	48	1,530,000	85

[a] Reagents and conditions: Ru 1.5×10^{-6} mol, 288 K, O_2 101.3 kPa. [b] In the oxidation of glutaraldehyde with two aldehyde moieties mono- and di-acids were observed, and the summation of the selectivity of the both products was 95%. [c] Ru 4.2×10^{-7} mol, 288−300 K. [d] Ru 4.2×10^{-7} mol.

the epoxidation conditions in the presence of IBA and O_2, their catalytic performances were completely different (Table 3). The supported Ru complex (**C**) transformed to the active unsaturated Ru complex (**D**) under the catalytic reaction conditions, while the homogeneous Ru precursor (**A**) aggregated to form precipitates under the catalytic reaction conditions, leading to a loss of its catalytic activity. The addition of SiO_2 into the homogeneous phase of (**A**) did not improve the deactivation of (**A**), which indicates that the chemical grafting on the SiO_2 surface and site-isolation are the key issue to preserve the active species for the selective oxidation.

We carried out the catalytic oxidations of various aldehyde compounds on the supported Ru catalyst (**D**), whose results are summarized in Table 4. 1-Butanal (*n*-butyraldehyde), 1-heptanal, 1-octanal, 1-decanal, and 1-dodecanal, which were linear aldehydes, selectively converted to their corresponding carboxylic acids with the selectivity of 88−100%. The TON of a conjugated benzaldehyde was 122 after 24 h with the acid selectivity of 100%. Both *p*-chlorobenzaldehyde and 2,6-dichlorobenzaldehyde with electron-withdrawing groups were less active than no-substituent benzaldehyde.

Huge turnover numbers could be achieved on the supported Ru catalyst (**D**) as shown in Table 4. The 38,800,000 equivalent of IBA (1.11 kg) was oxidized with the selectivity of 94% using 10 mg of the supported Ru catalyst (**D**) (TON was so tremendous as 38,800,000). TONs for 1-heptanal and 3-phenylpropionaldehyde oxidations were also so large as 31,500,000 and 1,530,000, respectively. Thus, the synthesized Ru complex on SiO_2 (**D**) was tremendously active for the selective oxidation of aldehyde compounds using O_2. Heteropolyacids with Ni, Co, Mn, and Cu,[33] supported Au catalysts,[34] and Y complexes[35] were reported to be so active for the aldehyde oxidation, but their TONs were less than 1000. Our supported Ru-monomer complex (**D**) provides the tremendous catalysis for the selective oxidation of aldehydes, showing remarkable TONs and TOFs. Furthermore, the SiO_2-supported catalyst (**D**) could be recycled by simple filtration though there was a drop of 6% in the selectivity between the first and second runs, while the conversion did not decrease as shown in Figure 3a. The reason of the drop is not clear at moment, but no leaching of the Ru complex was observed on the supported Ru catalyst (**D**) under the present reaction conditions and after the five-times recycled reactions, as characterized by XRF and ICP. Both the conversion and selectivity were still constant for runs 2−5 (Figure 3a), while the oxidation in the solution phase of the filtration did not occur.

3.3. Selective Epoxidation of Alkenes Using IBA/O_2. Highly efficient epoxidation of alkenes using a combination system of molecular oxygen and aldehyde on Ni^{2+} complex was reported

(33) Sloboda-Ronzner, D.; Neimann, K.; Neumann, R. *J. Mol. Catal.* **2007**, *262*, 109.
(34) Biella, S.; Prati, L.; Rossi, M. *J. Mol. Catal.* **2003**, *197*, 207.
(35) Roesky, P. W.; Canseco-Melchor, G.; Zulys, A. *Chem. Commun.* **2004**, 738.

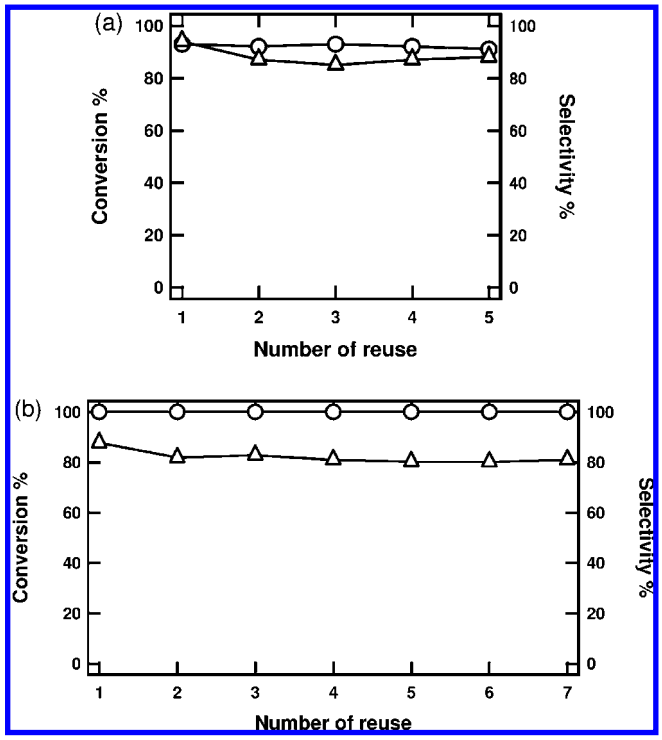

Figure 3. Conversion (○) and selectivity (Δ) in the recycling of the supported Ru catalyst (**D**). (a) IBA oxidation (Ru 0.4 wt %, Ru 6.0×10^{-6} mol, CH_2Cl_2 12 mL, 288 K, O_2 101.3 kPa, Ru/IBA = 1/200, 4 h). (b) *trans*-Stilbene epoxidation (Ru 2.7 wt %, Ru 1.0×10^{-5} mol, CH_2Cl_2 5 mL, 298 K, O_2 101.3 kPa, Ru/*trans*-stilbene/IBA = 1/100/100, 48 h).

by T. Yamada et al.[36] and selective oxidation (e.g., epoxidation, Baeyer−Villiger oxidation) using a combination system of molecular oxygen and aldehyde was well studied on various catalysts.[37−43] The supported Ru complex (**D**) with the unsaturated Ru site acted as an active site for the selective catalytic epoxidation of *trans*-stilbene using IBA and O_2 as reported previously as a communication.[15]

It was found that the surface Ru complex (**D**) exhibited unique catalytic performances for the selective epoxidation of not only *trans*-stilbene but also other alkenes with IBA/O_2. On the other hand, homogeneous $Ru(NH_3)_6Cl_3$, $Ru(bpy)Cl_2$ with both nitrogen and chlorine ligands, $Ru_2(p\text{-cymene})_2Cl_4$, and $RuCl_3$ never catalyzed the epoxidation of *trans*-stilbene with any oxidants such as O_2, H_2O_2, PhIO, or O_2/IBA. The Ru-precursor complex (**A**) produced a small amount of *trans*-stilbene oxide with PhIO or O_2/IBA, but the epoxidation stopped in a little while, forming black precipitates. The addition of SiO_2 into the homogeneous solution of (**A**) did not give any positive effect for the catalytic performance of the epoxidation (Table 5). Site-isolation on surfaces often creates efficient catalysis at the surfaces[44−46] and the site-isolation of the Ru complex was critical to maintain the catalytic activity for the selective epoxidation. The reaction with H_2O_2 on the surface Ru complex (**D**) was performed under a two-phase reaction condition, but we could not find any activity for the oxidation reaction. A reason may be due to the immiscible solvent condition. In the case of *tert*-butyl hydroperoxide (TBHP) in a *n*-heptane solution, conversion was similar to that of *m*-CPBA and epoxide selectivity was less than 40%. It is to be noted that the exclusive catalytic oxidation of IBA itself was suppressed during the selective alkene epoxidation. During the catalytic epoxidation of alkenes, coexisting IBA converted to isobutyric acid stoichiometrically, and the facile oxidation of sole IBA was not observed; that is, the amount of the acid product was stoichiometric to that of the epoxide product as shown in Figure 4. This means that the coexisting alkenes completely suppressed the facile catalytic oxidation of IBA itself with O_2.

The supported Ru complex (**D**) exhibited the good catalytic performances for the alkene epoxidation with 83−90% selectivity to epoxides under the O_2/IBA reaction conditions as shown in Table 5. Benzaldehyde (10−15%) was observed as a byproduct, and its diol and ester compounds were not observed. Other oxidants PhIO and *m*-chloroperbenzoic acid (*m*-CPBA) were poor oxidants with low conversion (30 and 46%, respectively) and low epoxide selectivity (16 and 41%, respectively). In the case of *cis*-stilbene epoxidation, *cis*-stilbene epoxide was only the product and no *trans*-stilbene epoxide was observed on the Ru catalyst (**D**). Benzaldehyde (24%) was observed as a byproduct. Cyclopentene, cyclohexene, and cyclooctene epoxidation also proceeded readily, and 1-hexene, 1-octene, and 1-decene, which are terminal alkenes, also converted to their corresponding epoxides on (**D**) (Table 5).

We also investigated large-scale catalytic epoxidation on the supported Ru catalyst (**D**), whose results are also listed in Table 5. In the case of *trans*-stilbene, we found a large TON of 2,100,000 with the selectivity of 90% after 168 h at 298 K, consuming the equivalent amount of IBA. The selective epoxidation of cyclopentene and norbornene showed TONs of 1,020,000 and 234,000, respectively (Table 5). The supported Ru catalyst (**D**) can be reused without any significant loss of the catalytic activity (100% conversion) seven times as shown in Figure 3b, indicating the high durability of the unsaturated active Ru complex supported on SiO_2 (**D**). There was a drop of 6% in the selectivity between the first and second runs, while the conversion of 100% did not decrease as shown in Figure 3b. The reason for the drop is not clear at moment, but no leaching of the Ru complex was observed on the supported Ru catalyst (**D**) under the present reaction conditions after the seven times recycled reactions, as characterized by XRF and ICP, and no change in the structural parameters for the supported Ru complexes was detected by XAFS analysis. Both the conversion and selectivity were still constant for runs 2−7 (Figure 3b), while the oxidation in the solution phase of the filtration did not occur.

(36) Yamada, T.; Takai, T.; Rhode, O.; Mukaiyama, T. *Chem. Lett.* **1991**, 1.
(37) Habor, J.; Mlodnicka, T.; Poltowicz, J. *J. Mol. Catal.* **1989**, *54*, 451.
(38) Rodgers, K. R.; Arafa, I. M.; Goff, H. M. *J. Chem. Soc., Chem. Commun.* **1990**, 1323.
(39) Takai, T.; Hata, E.; Yamada, T.; Mukaiyama, T. *Bull. Chem. Soc. Jpn.* **1991**, *64*, 2513.
(40) Murahashi, S.-I.; Oda, Y.; Naota, T. *J. Am. Chem. Soc.* **1992**, *114*, 7913.
(41) Mukaiyma, T.; Yamada, T.; Nagata, T.; Imagawa, K. *Chem. Lett.* **1993**, 327.
(42) Imagawa, K.; Nagata, T.; Yamada, T.; Mukaiyama, T. *Chem. Lett.* **1994**, 527.
(43) Kaneda, K.; Ueno, S.; Imanaka, T. *J. Mol. Catal. A: Chem.* **1995**, *102*, 135.
(44) Joubery, J.; Delbecq, F.; Sautet, P.; Le Roux, E.; Taofik, M.; Thieuleux, C.; Blanc, F.; Coperet, C.; Thivolle-Cazat, J.; Basset, J. M. *J. Am. Chem. Soc.* **2006**, *128*, 9157.
(45) Barbaro, P.; Bianchini, C.; Dal Santo, V.; Meli, A.; Moneti, S.; Psaro, R.; Scaffidi, A.; Sordelli, L.; Vizza, F. *J. Am. Chem. Soc.* **2006**, *128*, 7065.
(46) Kruithof, C. A.; Casado, M. A.; Guilena, G.; Egmond, M. R.; van der Kerk-van Hoof, A.; Heck, J. R. A.; Gebbink, J. M. K.; van Koten, G. *Chem.—Eur. J.* **2005**, *11*, 6869.

Table 5. Catalytic Performances for Alkene Epoxidation[a] on the Ru-Complex Catalysts (**A**) and (**D**)

catalyst	reactant	[alkene]/M	Ru/alkene/IBA	oxidant[b]	time/h	TON	epoxide selectivity/%
(**A**)	*trans*-stilbene	0.1	1/50/50	IBA/O_2	72	5	71
(**A**) + SiO_2[c]	*trans*-stilbene	0.1	1/50/50	IBA/O_2	72	5	66
(**D**)	*trans*-stilbene	0.1	1/50/0	O_2	72	0	0
(**D**)	*trans*-stilbene	0.1	1/50/0	H_2O_2[d,e]	72	0	0
(**D**)	*trans*-stilbene	0.1	1/50/0	PhIO[d]	72	15	16
(**D**)	*trans*-stilbene	0.1	1/50/0	*m*-CPBA[d]	48	23	41
(**D**)	*trans*-stilbene[b]	0.1	1/50/50	IBA/O_2	4	50	83
(**D**)	*trans*-stilbene[b]	0.2	1/100/100	IBA/O_2	12	100	88
(**D**)	*trans*-stilbene[b,f]	0.8	1/1000/1000	IBA/O_2	4	1000	90
(**D**)	*trans*-stilbene[g]	0.8	$1/2 \times 10^7/2 \times 10^7$	IBA/O_2	168	2100000	90
(**D**)	*cis*-stilbene	0.1	1/50/50	IBA/O_2	12	45	73
(**D**)	cyclopentene	0.1	1/50/50	IBA/O_2	48	43	82
(**D**)	cyclopentene[g]	5.0	$1/2 \times 10^6/2 \times 10^6$	IBA/O_2	240	1020000	80
(**D**)	cyclohexene	0.1	1/50/50	IBA/O_2	48	27	65
(**D**)	cyclooctene	0.1	1/50/50	IBA/O_2	48	49	81
(**D**)	styrene	0.1	1/50/50	IBA/O_2	48	25	38
(**D**)	1-hexene	0.1	1/50/50	IBA/O_2	96	29	67
(**D**)	1-octene	0.1	1/50/50	IBA/O_2	96	27	69
(**D**)	1-decene	0.1	1/50/50	IBA/O_2	96	29	82
(**D**)	norbornene	0.1	1/50/50	IBA/O_2	48	50	74
(**D**)	norbornene[g]	4.0	$1/2 \times 10^6/2 \times 10^6$	IBA/O_2	384	234000	87

[a] Reagents and conditions: Ru 1.0×10^{-5} mol, CH_2Cl_2 5 mL, 298 K, O_2 101.3 kPa. Catalyst (**D**) Ru 2.7 wt %. [b] In the *trans*-stilbene epoxidation by IBA/O_2 benzaldehyde was a major byproduct (about 10−15%). Other minor byproducts were benzylalcohol and benzoic acid. Diol and ester were not detected. In the use of PhIO and *m*-CPBA as oxidants, lots of benzaldehyde and benzoic acid were produced as byproducts. In the case of cyclohexene epoxidation, cyclohexenone (15%) and cyclohexenol (20%) were observed as byproducts. [c] SiO_2 40 mg. [d] *trans*-Stilbene/oxidant = 1/1. [e] Two-phase reaction. [f] CH_2Cl_2 12 mL. [g] Catalyst (**D**) Ru 0.4 wt %, Ru 4.2×10^{-7} mol, 288 K, O_2 101.3 kPa.

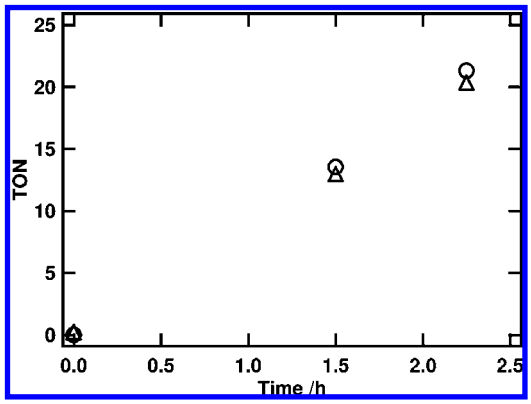

Figure 4. TONs of *trans*-stilbene oxide and isobutyric acid for the epoxidation of *trans*-stilbene on the supported Ru catalyst (**D**) (Ru 2.7 wt %) at 303 K. ○: *trans*-Stilbene and Δ: IBA. Ru 2.7×10^{-6} mol, CH_2Cl_2 3 mL, O_2 101.3 kPa, Ru/*trans*-stilbene/IBA=1/100/100.

The reaction mechanism of epoxidation using the combination system of molecular oxygen and aldehyde was investigated, and several reaction mechanisms and active oxygen species were proposed.[47−51] Autooxidation in the absence of metal species proceeds, and the stereoselective epoxidation of 5,6-double bond in cholesteryl benzoate (eq 1) clearly shows whether metal species is concerned in epoxidation.[31]

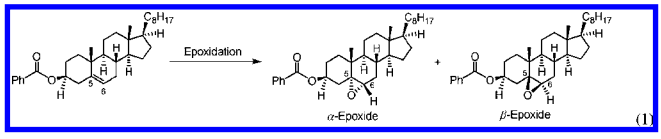

We investigated the epoxidation (eq 1) using *m*-chloroperbenzoic acid (*m*-CPBA) and the supported Ru catalyst (**D**), whose steroselectivities were opposite. In the case of *m*-CPBA, autooxidation pathway takes place in epoxidation, α-epoxide was preferably produced and the product ratio of α-epoxide/*β*-epoxide was 70/30, which agreed with the reported result.[31] On the other hand, the product ratio of α-epoxide/*β*-epoxide was found to be 21/79 (3 h, conv. 16%) and 22/78 (24 h, conv. 67%) on the supported Ru catalyst (**D**). Judging from the *β*-selective epoxidation of cholesteryl benzoate, we can say with safety that the *trans*-stilbene epoxidation is not autooxidation using free radical species in the solution and the supported Ru species positively participates in the catalytic epoxidation on the surface.

3.4. Reaction Mechanisms for the Alternative Selective Oxidation Pathways. We have found that the supported Ru complex (**D**) is highly active for both the IBA oxidation with O_2 and the *trans*-stilbene epoxidation with IBA/O_2 as mentioned above. The reaction rate of the IBA oxidation to isobutyric acid is much faster than that of *trans*-stilbene epoxidation to *trans*-stilbene oxide under the identical IBA/O_2 concentration for the both oxidations. Indeed, when the concentration of IBA was 0.1 M in CH_2Cl_2, the TOF (turnover frequency: equivalent to reaction rate) of the catalytic IBA oxidation with O_2 in the absence of *trans*-stilbene (IBA + O_2 → 2 isobutyric acid) was 138 h^{-1}, while the TOF of the catalytic *trans*-stilbene epoxidation with O_2 using IBA (0.1 M) (*trans*-stilbene + IBA + O_2 → *trans*-stilbene oxide + isobutyric acid) was 12 h^{-1}, where no catalytic oxidation of IBA alone with O_2 proceeded. The origin and mechanism of the both selective oxidation pathways and the switchover of the reaction pathways will be discussed below.

It is to be noted that the IBA/O_2 molecules were consumed for the epoxidation of *trans*-stilbene (*trans*-stilbene + IBA + O_2 → *trans*-stilbene oxide + isobutyric acid) and the much faster oxidation of IBA itself (2 IBA + O_2 → 2 isobutyric acid) in

(47) Nishida, Y.; Fujimoto, T.; Tanaka, N. *Chem. Lett.* **1992**, 1291.
(48) Simmons, K. E.; van Sickle, D. E. *J. Am. Chem. Soc.* **1973**, *95*, 7759.
(49) Diaz, R. R.; Selby, K.; Waddington, D. J. *J. Chem. Soc., Perkin Trans. 2* **1975**, 758.
(50) Simandi, L. I., Ed. *Catalytic Activation of Dioxygen by Metal Complexes*; Kluwer Academic Publishers: Dordrecht, The Netherlands, 1992; pp 318−331.
(51) Sheldon, R. A., Kochi, J. K., Eds. *Metal-Catalyzed Oxidations of Organic Compounds*; Academic Press: New York, 1981; pp 359−363.

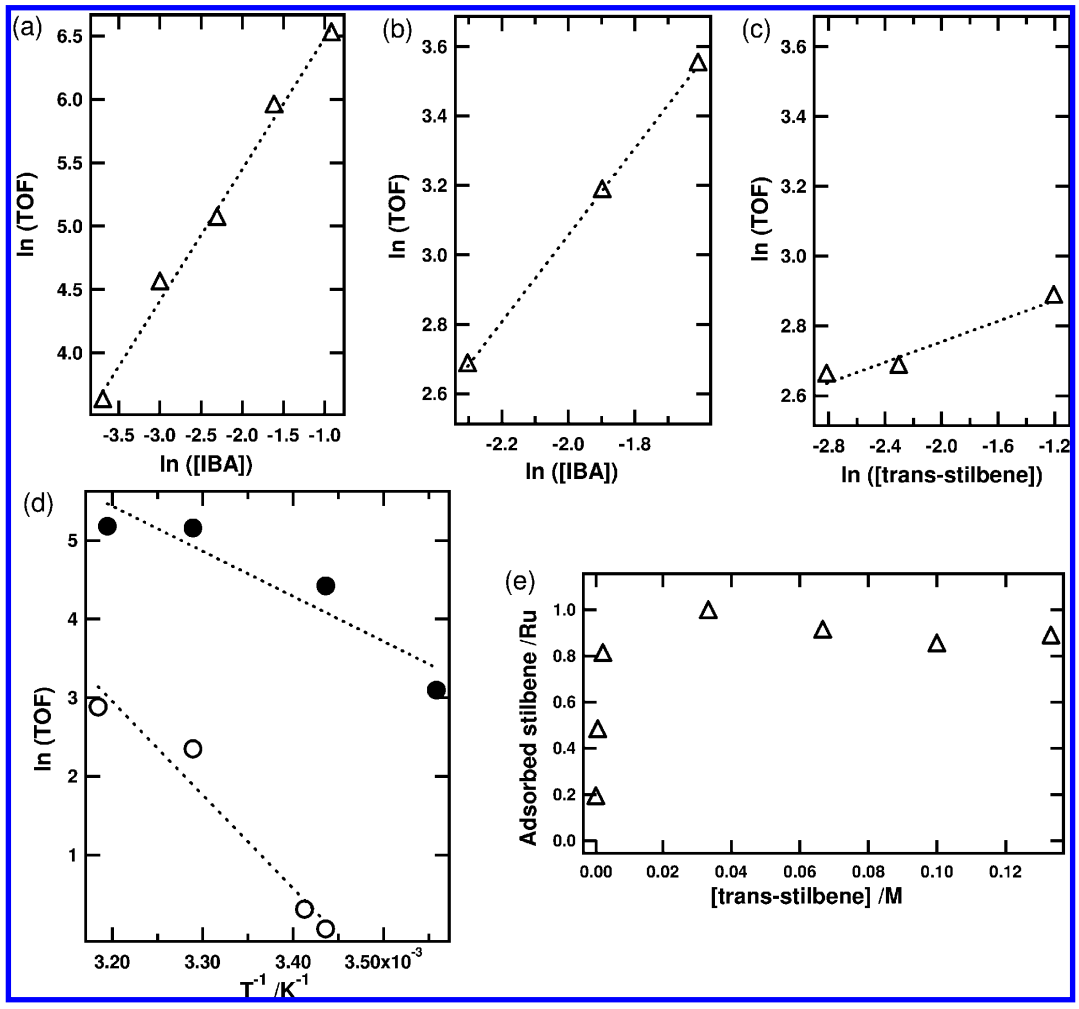

Figure 5. (a) Reaction order to IBA concentration in the IBA oxidation on (**D**) (Ru 0.4 wt %, Ru 4.2×10^{-7} mol, 288 K). (b) Reaction order to IBA concentration in the *trans*-stilbene epoxidation on (**D**) (Ru 0.4 wt %, Ru 4.2×10^{-7} mol, 314 K, [*trans*-stilbene] = 0.1 M). (c) Reaction order to *trans*-stilbene concentration in the *trans*-stilbene epoxidation on (**D**) (Ru 0.4 wt %, Ru 4.2×10^{-7} mol, 314 K, [IBA] = 0.1 M). (d) Arrhenius plots for the IBA oxidation (○, [IBA] = 0.1 M) and the *trans*-stilbene epoxidation (●, [IBA] = 0.1 M and [*trans*-stilbene] = 0.1 M) on (**D**) (Ru 2.7 wt %, Ru 2.7×10^{-6} mol). (e) Amount of adsorbed *trans*-stilbene on (**D**) against the concentration of *trans*-stilbene at 298 K (Ru 2.7 wt %, Ru 2×10^{-5} mol, [IBA] = 0.1 M, N_2 atmosphere).

the presence of *trans*-stilbene was completely suppressed. Indeed the produced *trans*-stilbene epoxide and isobutyric acid were equivalent to each other from the initial stage of the epoxidation through the whole reaction period as shown in Figure 4. The addition of *trans*-stilbene switched over the reaction pathway of the much faster aldehyde oxidation to the much slower alkene epoxidation. Even if the excess amount of IBA compared to the amount of *trans*-stilbene existed in the reaction solution, the IBA sole oxidation without the alkene epoxidation did not proceed in the presence of alkene.

The kinetic parameters of the both selective oxidations on the supported Ru catalyst (**D**) were investigated to understand the alternative selective oxidation mechanism. As shown in Figure 5a, the reaction order to the IBA concentration was 1.04 for the IBA sole oxidation without any alkenes, and the activation energy was estimated to be 48 kJ mol^{-1} (Figure 5d). There was no peroxide species observed by the iodometric titration of the steady-state reaction solution after the filtration of the solid catalyst. The species (26% equivalent to Ru) capable of iodo-oxidation (e.g., peroxyacid, peroxide, metal−oxo, etc.)[52] was detected on the supported Ru catalyst separated from the reaction solution. These results indicate that IBA was oxidized to form active intermediate species with alkene oxidation activity on the supported Ru complex and IBA was not autooxidized in the reaction solution. The amount of the active intermediate species on the supported Ru complex (**D**) decreased to 12% of Ru quantity after the completion of the IBA oxidation reaction, indicating that the intermediates are labile.

In the case of the *trans*-stilbene epoxidation, the similar results on iodometric titration were observed and the opposite selectivity in the stereoselective epoxidation of cholesteryl benzoate (α-epoxide and β-epoxide) was observed as mentioned in section 3.3, which exclude the possibility of the autooxidation mechanism on the supported Ru catalyst.[31] The reaction orders with respect to IBA and *trans*-stilbene were estimated to be 1.25 and 0.15, respectively, as shown in b and c of Figure 5. The activation energy of the epoxidation was 99 kJ mol^{-1} (Figure 5d), which was about twice that of the IBA oxidation (48 kJ mol^{-1}). The activation energies of the epoxidation of limonene with a terminal C=C bond and an internal C=C bond were 81 kJ mol^{-1} and 61 kJ mol^{-1}, respectively. The different activation energies for the terminal and internal C=C bond in limonene and the small reaction order to *trans*-stilbene demonstrate that *trans*-stilbene as a strong adsorbed species on the Ru center is

(52) Cook, G. K.; Mayer, J. M. *J. Am. Chem. Soc.* **1994**, *116*, 1855.

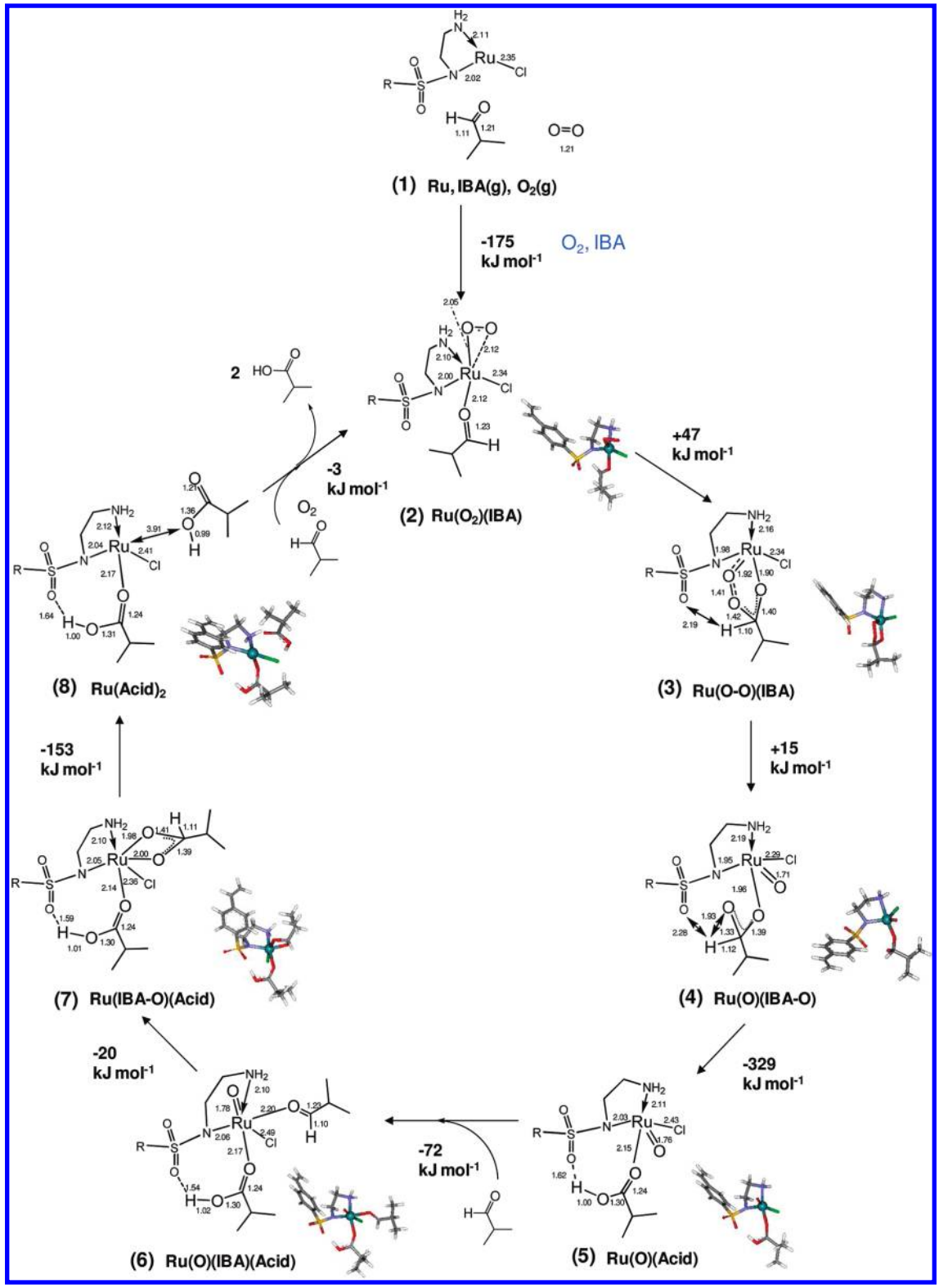

Figure 6. Reaction pathway of the selective IBA oxidation and the intermediate structures calculated by hybrid DFT. Acid: isobutyric acid. Blue: Ru, red: O, green: Cl, yellow: S, gray: C, and white: H.

involved in the rate-determining step of the epoxidation, where most of Ru sites are coordinated by *trans*-stilbene at the steady-state reaction.

Indeed, *trans*-stilbene preferentially adsorbed on the unsaturated active Ru complex (**D**) in the presence of the equivalent amount of IBA. Figure 5e shows the amounts of adsorbed *trans*-stilbene per Ru against the concentration of *trans*-stilbene in the presence of IBA under N_2 atmosphere. It was found that *trans*-stilbene preferably adsorbed on the unsaturated Ru centers (**D**) and the adsorption saturated at the nearly equivalent amount to Ru as shown in Figure 5e. The preferable coordination of alkenes onto the Ru sites may induce the switchover of the selective oxidation pathways from the facile aldehyde oxidation to the hard epoxidation.

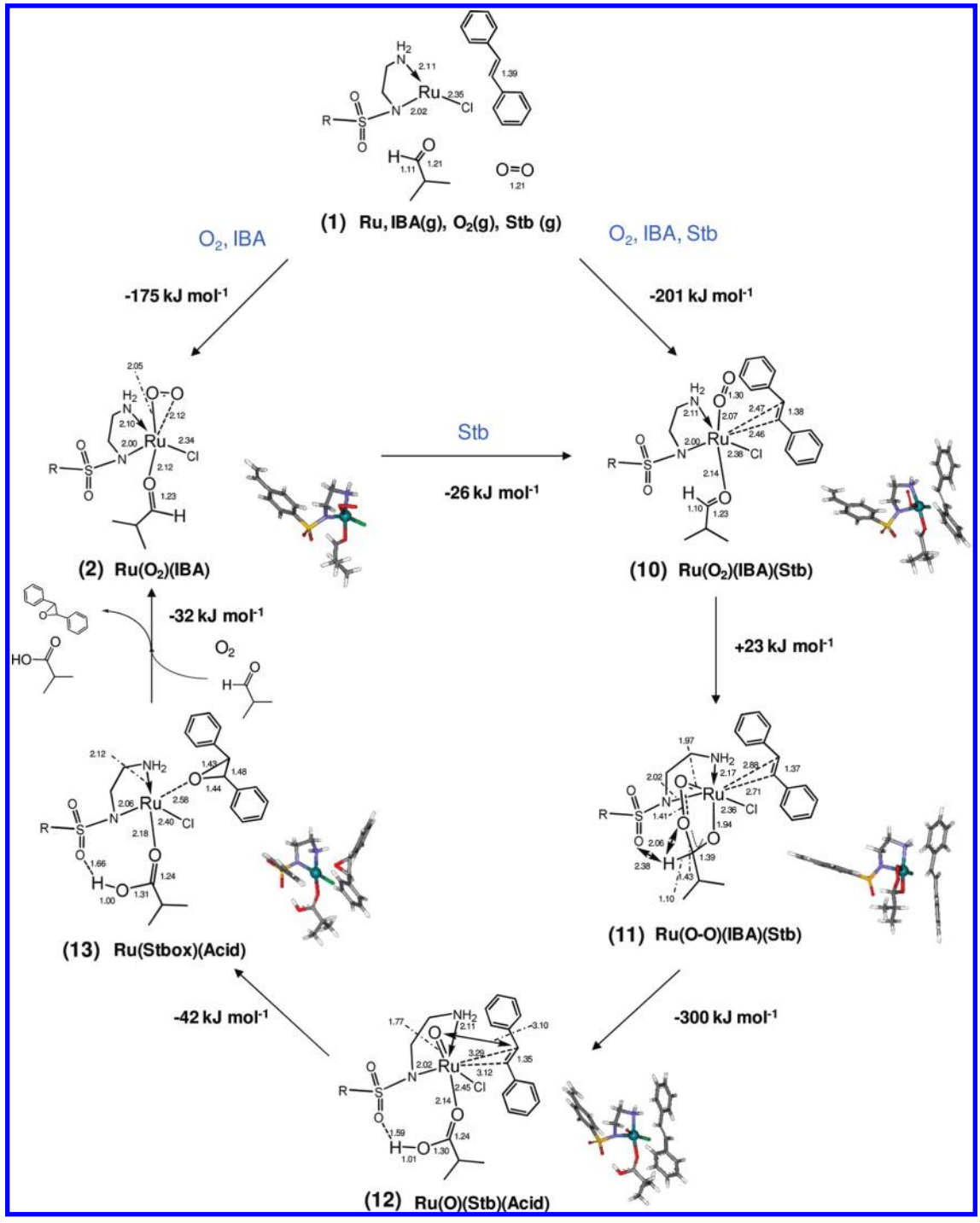

Figure 7. Reaction pathway of the *trans*-stilbene epoxidation and the intermediate structures calculated by hybrid DFT. Stb: *trans*-stilbene, Stbox: *trans*-stilbene oxide, and Acid: isobutyric acid. Blue: Ru, red: O, green: Cl, yellow: S, gray: C, and white: H.

We investigated the energy profiles of the reaction pathways for the IBA sole oxidation with O_2 in the absence of *trans*-stilbene and the IBA-assisted *trans*-stilbene epoxidation with O_2 on the surface Ru complex (**D**) by DFT calculations. The calculated energy profiles of the IBA sole oxidation with O_2 and the *trans*-stilbene epoxidation with IBA/O_2 are shown in Supporting Information 1, where the relative energy profiles in the same spin states would be valid to discuss on the reaction pathways. The structures of the reaction intermediates and the transition states are also illustrated in Supporting Information 2, 3 and 4, respectively. On the basis of the energy profiles the reaction pathways for the catalytic IBA oxidation and the catalytic *trans*-stilbene oxidation are shown in Figure 6 and Figure 7, respectively.

In the IBA sole oxidation, both IBA and O_2 coordinate to the unsaturated Ru complex (**1**) to form species (**2**) with an energy barrier of 57 kJ mol^{-1} as shown in Figure 6 and Supporting Information 1. The first-order kinetics to the IBA concentration with the activation energy of 48 kJ mol^{-1} is attributed to the rate-limiting O_2 addition to the aldehyde carbon to form species (**3**) with elongated O_2, which is followed by the transformation of (**3**) to an intermediate (**5**) with Ru═O via species (**4**) with Ru═O. The species (**5**) further reacts with the second IBA to produce the corresponding acids via species (**6**),

(**7**), and (**8**). The Ru═O groups were successfully detected by iodometry in the steady-state oxidation (26% of the stoichiometric amount of Ru).

On the other hand, we observed the nearly stoichiometric adsorption of *trans*-stilbene on the Ru site (**D**) in Figure 5e, which implies that the majority of Ru sites exists as the species coordinated with *trans*-stilbene in the selective oxidation of *trans*-stilbene. The adsorption energy of *trans*-stilbene on Ru sites was estimated to be 93 kJ mol^{-1} by DFT calculations, and the obtained Ru(*trans*-stilbene) species is further coordinated with O_2 and IBA to form species (**10**) in Figure 7. Alternatively, *trans*-stilbene coordinates to species (**2**) to form the species (**10**). The species (**10**) transforms to species (**11**) and to an intermediate (**12**) with Ru═O via double cascades. The epoxidation occurs by the rate-limiting addition of the Ru═O oxygen to the C═C bond of *trans*-stilbene with an energy barrier of 98 kJ mol^{-1} in the step from (**12**) to (**13**). This agrees with the observed activation energy of 99 kJ mol^{-1} for the catalytic *trans*-stilbene epoxidation with IBA/O_2. The energy profile of the reaction pathways may explain the nearly stoichiometric adsorption of *trans*-stilbene on the Ru site as species (**12**), and it is also compatible with the kinetics proportional to the IBA concentration and nearly independent of the *trans*-stilbene concentration. It should be noted that the present DFT calculations for the transition states such as TS(**10**−**11**) and TS(**11**−**12**) may involve certain values of error bars.

Thus, we can document how the alternative selective oxidation pathways are switched over from the facile rapid aldehyde oxidation with the lower activation energy to the harder alkene epoxidation with the higher activation energy by the existence of alkenes. The important issue for the selective catalytic epoxidation of *trans*-stilbene with IBA/O_2 without the catalytic IBA oxidation with O_2 is the coordination of *trans*-stilbene on the Ru center, which makes it possible to efficiently rearrange the bonds of the three coordinated reactants (*trans*-stilbene + IBA + O_2) on the Ru center to form the species (**12**) via the species (**10**) and (**11**) in the coordination sphere. As a result, the IBA sole oxidation is suppressed due to a negligible concentration of the species (**2**). The coordination of the second IBA to the species (**2**) to form species (**9**) decreases the IBA oxidation rate by self-poisoning due to appearance of the higher energy barrier for the IBA oxidation (Supporting Information 1). The unsaturated Ru-complex structure (**D**) immobilized at the SiO_2 surface, which is obtained by *p*-cymene elimination in couple with the exothermic IBA + O_2 reaction, is crucial to provide the efficient reaction pathways involving the Ru^{4+}═O species active for both selective aldehyde oxidation (TON of IBA oxidation: 38,800,000) and alkene epoxidation (TON of *trans*-stilbene epoxidation: 2,100,000). This aspect gives insight into the origin of the efficient catalysis for selective epoxidation of alkenes with IBA/O_2.

4. Conclusions

The SiO_2-supported unsaturated Ru-monomer complex, which was prepared the energy-gaining way by using IBA and O_2, exhibited tremendous TONs and TOFs for the selective oxidation catalyzes of the aldehyde oxidation and the alkene epoxidation at ambient temperature. The TONs of 38,800,000 for the IBA oxidation (TOF: 1600 s^{-1}) and 2,100,000 for the *trans*-stilbene epoxidation (TOF: 6 s^{-1}) were achieved, and the active Ru-complex catalyst (**D**) could be reusable without any significant loss of its catalytic activities. We found that the addition of alkenes switched over the selective oxidation pathways from the fast IBA sole oxidation to the harder slow alkene epoxidation, suppressing the facile IBA sole oxidation, due not only to the occupation of a vacant site on the Ru center by *trans*-stilbene but also to the facile conformation and bond rearrangements of IBA, O_2, and alkene in the coordination sphere. The unsaturated Ru-complex structure isolatedly at the SiO_2 surface was crucial to provide the selective oxidation catalysis via the adsorption of plural reactants in the same coordination sphere.

Acknowledgment. The work was supported by a Grant-in-Aid for Scientific Research on Priority Areas (No. 18065003) and a Grant-in-Aid for Scientific Research (S) (No. 18106013) from MEXT, an Inoue Science Research Award from Inoue Foundation for Science, and a JCII Subsidy System for Advanced Innovation in Chemical Industry. XAFS measurements were performed by the approval of PF-PAC (Nos. 2005G209 and 2008G154).

Supporting Information Available: Energy diagram for the selective oxidation reactions calculated by hybrid DFT, the intermediate structures in the IBA oxidation calculated by hybrid DFT, the intermediate structures in the *trans*-stilbene oxidation calculated by hybrid DFT, the structures of the transition states calculated by hybrid DFT, and complete reference 24. This information is available free of charge via the Internet at http://pubs.acs.org.

JA9079513